

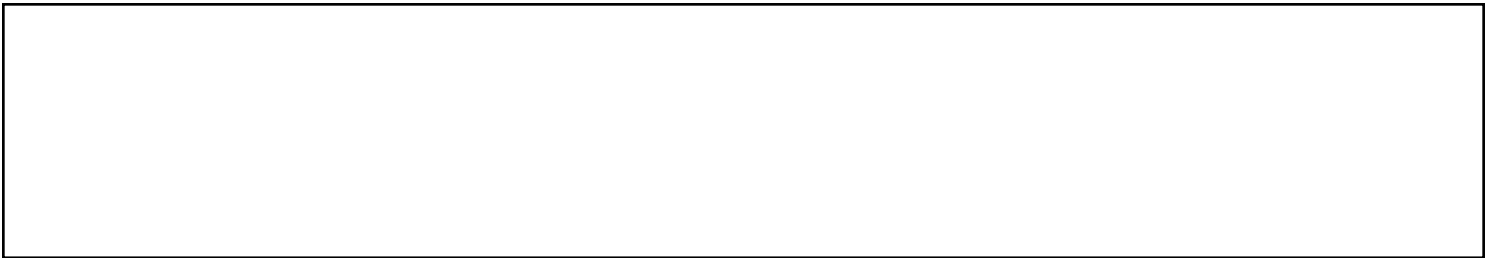
POLITECNICO DI TORINO  
Repository ISTITUZIONALE

Sensitivity of future liquid argon dark matter search experiments to core-collapse supernova neutrinos

Original

Sensitivity of future liquid argon dark matter search experiments to core-collapse supernova neutrinos / Agnes, P.; Albergo, S.; Albuquerque, I. F. M.; Alexander, T.; Alici, A.; Alton, A. K.; Amaudruz, P.; Arcelli, S.; Ave, M.; Avetissov, I. Ch.; Avetisov, R. I.; Azzolini, O.; Back, H. O.; Balmforth, Z.; Barbarian, V.; Barrado Olmedo, A.; Barrillon, P.; Basco, A.; Batignani, G.; Bondar, A.; Bonivento, W. M.; Borisova, E.; Bottino, B.; Boulay, M. G.; Buccino, G.; Bussino, S.; Busto, J.; Buzulutskov, A.; Cadeddu, M.; Cadoni, M.; Caminata, A.; Canci, N.; Cappello, G.; Caravati, M.; Cárdenas-Montes, M.; Carlini, M.; Carnesecchi, F.; Castello, P.; Catalanotti, S.; Cataudella, V.; Cavalcante, P.; Cavuoti, S.; Cebrian, S.; Cela Ruiz, J. M.; Celano, B.; Chashin, S.; Chepurnov, A.; Cicalò, C.; Cifarelli, L.; Cintas, D.; Coccetti, F.; Cocco, V.; Colocci, M.; Conde Vilda, E.; Consiglio, L.; Copello, S.; Covone, G.; Czudak, P.; D'Auria, S.; Da Rocha Rolo, M. D.; Dadoun, O.; Daniel, M.; Davini, S.; De Candia, A.; De Cecco, S.; De Falco, A.; De Filippis, G.; De Gruttola, D.; De Guido, G.; De Rosa, G.; Della Valle, M.; Dellacasa, G.; De Pasquale, S.; Derbin, A. V.; Devoto, A.; Di Noto, L.; Dionisi, C.; Di Stefano, P.; Dolganov, G.; Dördei, F.; Downing, M.; Erjavec, T.; Fernandez Diaz, M.; Fiorillo, G.; Franceschi, A.; Franco, D.; Frolov, E.; Funicello, N.; Gabriele, F.; Galbiati, C.; Garbini, M.; Garcia Abia, P.; Gendotti, A.; Ghiano, C.; Giampaolo, R.; Giordano, C.; Giorgi, M. A.; Giovanetti, G. K.; Goicoechea Casanueva, V.; Gola, A.; Graciani Diaz, R.; Grigoriev, G. Y.; Golob, T.; Gori, G.; Gouveia, J. M.; Guadagnoli, M.; Gulino, M.; Guo, C.; Hackett, B. R.; Hallin, A.; Haranczyk, M.; Hill, S.; Horikawa, S.; Hubaut, F.; Hugues, T.; Hungerford, E. V.; Ianni, An.; Ippolito, V.; James, C. C.; Jillings, C.; Kachru, P.; Kemp, A. A.; Kendziora, C. L.; Keppel, G.; Khomyakov, A. V.; Kim, S.; Kish, A.; Kochanek, I.; Kondo, K.; Korga, G.; Kubankin, A.; Kugathasan, R.; Kuss, M.; Kuniak, M.; La Commara, M.; Lai, M.; Langrock, S.; Leyton, M.; Li, X.; Lidey, L.; Lissia, M.; Longo, G.; Machulin, I. N.; Mapelli, L.; Marasciulli, A.; Margotti, A.; Mari, S. M.; Maricic, J.; Martinez, M.; Martin, R.; Roman De Davila, M.; Mattheucci, M.; Masian, A.; Mazzini, A.; Mészáros, A. B.; Mészáros, J.; Mészáros, P.; Mészáros, D.; Mészáros, L.; Mészáros, S.; Mészáros, E.; Mészáros, A.; Mészáros, B.; Mészáros, C.; Mészáros, D.; Mészáros, E.; Mészáros, F.; Mészáros, G.; Mészáros, H.; Mészáros, I.; Mészáros, J.; Mészáros, K.; Mészáros, L.; Mészáros, M.; Mészáros, N.; Mészáros, O.; Mészáros, P.; Mészáros, Q.; Mészáros, R.; Mészáros, S.; Mészáros, T.; Mészáros, U.; Mészáros, V.; Mészáros, W.; Mészáros, X.; Mészáros, Y.; Mészáros, Z.; Mészáros, AA.; Mészáros, AB.; Mészáros, AC.; Mészáros, AD.; Mészáros, AE.; Mészáros, AF.; Mészáros, AG.; Mészáros, AH.; Mészáros, AI.; Mészáros, AJ.; Mészáros, AK.; Mészáros, AL.; Mészáros, AM.; Mészáros, AN.; Mészáros, AO.; Mészáros, AP.; Mészáros, AQ.; Mészáros, AR.; Mészáros, AS.; Mészáros, AT.; Mészáros, AU.; Mészáros, AV.; Mészáros, AW.; Mészáros, AX.; Mészáros, AY.; Mészáros, AZ.; Mészáros, BA.; Mészáros, BB.; Mészáros, BC.; Mészáros, BD.; Mészáros, BE.; Mészáros, BF.; Mészáros, BG.; Mészáros, BH.; Mészáros, BI.; Mészáros, BJ.; Mészáros, BK.; Mészáros, BL.; Mészáros, BM.; Mészáros, BN.; Mészáros, BO.; Mészáros, BP.; Mészáros, BQ.; Mészáros, BR.; Mészáros, BS.; Mészáros, BT.; Mészáros, BU.; Mészáros, BV.; Mészáros, BW.; Mészáros, BX.; Mészáros, BY.; Mészáros, BZ.; Mészáros, CA.; Mészáros, CB.; Mészáros, CC.; Mészáros, CD.; Mészáros, CE.; Mészáros, CF.; Mészáros, CG.; Mészáros, CH.; Mészáros, CI.; Mészáros, CJ.; Mészáros, CK.; Mészáros, CL.; Mészáros, CM.; Mészáros, CN.; Mészáros, CO.; Mészáros, CP.; Mészáros, CQ.; Mészáros, CR.; Mészáros, CS.; Mészáros, CT.; Mészáros, CU.; Mészáros, CV.; Mészáros, CW.; Mészáros, CX.; Mészáros, CY.; Mészáros, CZ.; Mészáros, DA.; Mészáros, DB.; Mészáros, DC.; Mészáros, DD.; Mészáros, DE.; Mészáros, DF.; Mészáros, DG.; Mészáros, DH.; Mészáros, DI.; Mészáros, DJ.; Mészáros, DK.; Mészáros, DL.; Mészáros, DM.; Mészáros, DN.; Mészáros, DO.; Mészáros, DP.; Mészáros, DQ.; Mészáros, DR.; Mészáros, DS.; Mészáros, DT.; Mészáros, DU.; Mészáros, DV.; Mészáros, DW.; Mészáros, DX.; Mészáros, DY.; Mészáros, DZ.; Mészáros, EA.; Mészáros, EB.; Mészáros, EC.; Mészáros, ED.; Mészáros, EE.; Mészáros, EF.; Mészáros, EG.; Mészáros, EH.; Mészáros, EI.; Mészáros, EJ.; Mészáros, EK.; Mészáros, EL.; Mészáros, EM.; Mészáros, EN.; Mészáros, EO.; Mészáros, EP.; Mészáros, EQ.; Mészáros, ER.; Mészáros, ES.; Mészáros, ET.; Mészáros, EU.; Mészáros, EV.; Mészáros, EW.; Mészáros, EX.; Mészáros, EY.; Mészáros, EZ.; Mészáros, FA.; Mészáros, FB.; Mészáros, FC.; Mészáros, FD.; Mészáros, FE.; Mészáros, FF.; Mészáros, FG.; Mészáros, FH.; Mészáros, FI.; Mészáros, FJ.; Mészáros, FK.; Mészáros, FL.; Mészáros, FM.; Mészáros, FN.; Mészáros, FO.; Mészáros, FP.; Mészáros, FQ.; Mészáros, FR.; Mészáros, FS.; Mészáros, FT.; Mészáros, FU.; Mészáros, FV.; Mészáros, FW.; Mészáros, FX.; Mészáros, FY.; Mészáros, FZ.; Mészáros, GA.; Mészáros, GB.; Mészáros, GC.; Mészáros, GD.; Mészáros, GE.; Mészáros, GF.; Mészáros, GG.; Mészáros, GH.; Mészáros, GI.; Mészáros, GJ.; Mészáros, GK.; Mészáros, GL.; Mészáros, GM.; Mészáros, GN.; Mészáros, GO.; Mészáros, GP.; Mészáros, GQ.; Mészáros, GR.; Mészáros, GS.; Mészáros, GT.; Mészáros, GU.; Mészáros, GV.; Mészáros, GW.; Mészáros, GX.; Mészáros, GY.; Mészáros, GZ.; Mészáros, HA.; Mészáros, HB.; Mészáros, HC.; Mészáros, HD.; Mészáros, HE.; Mészáros, HF.; Mészáros, HG.; Mészáros, HH.; Mészáros, HI.; Mészáros, HJ.; Mészáros, HK.; Mészáros, HL.; Mészáros, HM.; Mészáros, HN.; Mészáros, HO.; Mészáros, HP.; Mészáros, HQ.; Mészáros, HR.; Mészáros, HS.; Mészáros, HT.; Mészáros, HU.; Mészáros, HV.; Mészáros, HW.; Mészáros, HX.; Mészáros, HY.; Mészáros, HZ.; Mészáros, IA.; Mészáros, IB.; Mészáros, IC.; Mészáros, ID.; Mészáros, IE.; Mészáros, IF.; Mészáros, IG.; Mészáros, IH.; Mészáros, II.; Mészáros, IJ.; Mészáros, IK.; Mészáros, IL.; Mészáros, IM.; Mészáros, IN.; Mészáros, IO.; Mészáros, IP.; Mészáros, IQ; Mészáros, IR; Mészáros, IS; Mészáros, IT; Mészáros, IU; Mészáros, IV; Mészáros, IW; Mészáros, IX; Mészáros, IY; Mészáros, IZ; Mészáros, JA; Mészáros, JB; Mészáros, JC; Mészáros, JD; Mészáros, JE; Mészáros, JF; Mészáros, JG; Mészáros, JH; Mészáros, JI; Mészáros, JJ; Mészáros, JK; Mészáros, JL; Mészáros, JM; Mészáros, JN; Mészáros, JO; Mészáros, JP; Mészáros, JQ; Mészáros, JR; Mészáros, JS; Mészáros, JT; Mészáros, JU; Mészáros, JV; Mészáros, JW; Mészáros, JX; Mészáros, JY; Mészáros, JZ; Mészáros, KA; Mészáros, KB; Mészáros, KC; Mészáros, KD; Mészáros, KE; Mészáros, KF; Mészáros, KG; Mészáros, KH; Mészáros, KI; Mészáros, KJ; Mészáros, KK; Mészáros, KL; Mészáros, KM; Mészáros, KN; Mészáros, KO; Mészáros, KP; Mészáros, KQ; Mészáros, KR; Mészáros, KS; Mészáros, KT; Mészáros, KU; Mészáros, KV; Mészáros, KW; Mészáros, KX; Mészáros, KY; Mészáros, KZ; Mészáros, LA; Mészáros, LB; Mészáros, LC; Mészáros, LD; Mészáros, LE; Mészáros, LF; Mészáros, LG; Mészáros, LH; Mészáros, LI; Mészáros, LJ; Mészáros, LK; Mészáros, LL; Mészáros, LM; Mészáros, LN; Mészáros, LO; Mészáros, LP; Mészáros, LQ; Mészáros, LR; Mészáros, LS; Mészáros, LT; Mészáros, LU; Mészáros, LV; Mészáros, LW; Mészáros, LX; Mészáros, LY; Mészáros, LZ; Mészáros, MA; Mészáros, MB; Mészáros, MC; Mészáros, MD; Mészáros, ME; Mészáros, MF; Mészáros, MG; Mészáros, MH; Mészáros, MI; Mészáros, MJ; Mészáros, MK; Mészáros, ML; Mészáros, MN; Mészáros, MO; Mészáros, MP; Mészáros, MQ; Mészáros, MR; Mészáros, MS; Mészáros, MT; Mészáros, MU; Mészáros, MV; Mészáros, MW; Mészáros, MX; Mészáros, MY; Mészáros, MZ; Mészáros, NA; Mészáros, NB; Mészáros, NC; Mészáros, ND; Mészáros, NE; Mészáros, NF; Mészáros, NG; Mészáros, NH; Mészáros, NI; Mészáros, NJ; Mészáros, NK; Mészáros, NL; Mészáros, NM; Mészáros, NO; Mészáros, NP; Mészáros, NQ; Mészáros, NR; Mészáros, NS; Mészáros, NT; Mészáros, NU; Mészáros, NV; Mészáros, NW; Mészáros, NX; Mészáros, NY; Mészáros, NZ; Mészáros, OA; Mészáros, OB; Mészáros, OC; Mészáros, OD; Mészáros, OE; Mészáros, OF; Mészáros, OG; Mészáros, OH; Mészáros, OI; Mészáros, OJ; Mészáros, OK; Mészáros, OL; Mészáros, OM; Mészáros, ON; Mészáros, OO; Mészáros, OP; Mészáros, OQ; Mészáros, OR; Mészáros, OS; Mészáros, OT; Mészáros, OU; Mészáros, OV; Mészáros, OW; Mészáros, OX; Mészáros, OY; Mészáros, OZ; Mészáros, PA; Mészáros, PB; Mészáros, PC; Mészáros, PD; Mészáros, PE; Mészáros, PF; Mészáros, PG; Mészáros, PH; Mészáros, PI; Mészáros, PJ; Mészáros, PK; Mészáros, PL; Mészáros, PM; Mészáros, PN; Mészáros, PO; Mészáros, PP; Mészáros, PQ; Mészáros, PR; Mészáros, PS; Mészáros, PT; Mészáros, PU; Mészáros, PV; Mészáros, PW; Mészáros, PX; Mészáros, PY; Mészáros, PZ; Mészáros, QA; Mészáros, QB; Mészáros, QC; Mészáros, QD; Mészáros, QE; Mészáros, QF; Mészáros, QG; Mészáros, QH; Mészáros, QI; Mészáros, QJ; Mészáros, QK; Mészáros, QL; Mészáros, QM; Mészáros, QN; Mészáros, QO; Mészáros, QP; Mészáros, QQ; Mészáros, QR; Mészáros, QS; Mészáros, QT; Mészáros, QU; Mészáros, QV; Mészáros, QW; Mészáros, QX; Mészáros, QY; Mészáros, QZ; Mészáros, RA; Mészáros, RB; Mészáros, RC; Mészáros, RD; Mészáros, RE; Mészáros, RF; Mészáros, RG; Mészáros, RH; Mészáros, RI; Mészáros, RJ; Mészáros, RK; Mészáros, RL; Mészáros, RM; Mészáros, RN; Mészáros, RO; Mészáros, RP; Mészáros, RQ; Mészáros, RR; Mészáros, RS; Mészáros, RT; Mészáros, RU; Mészáros, RV; Mészáros, RW; Mészáros, RX; Mészáros, RY; Mészáros, RZ; Mészáros, SA; Mészáros, SB; Mészáros, SC; Mészáros, SD; Mészáros, SE; Mészáros, SF; Mészáros, SG; Mészáros, SH; Mészáros, SI; Mészáros, SJ; Mészáros, SK; Mészáros, SL; Mészáros, SM; Mészáros, SN; Mészáros, SO; Mészáros, SP; Mészáros, SQ; Mészáros, SR; Mészáros, SS; Mészáros, ST; Mészáros, SU; Mészáros, SV; Mészáros, SW; Mészáros, SX; Mészáros, SY; Mészáros, SZ; Mészáros, TA; Mészáros, TB; Mészáros, TC; Mészáros, TD; Mészáros, TE; Mészáros, TF; Mészáros, TG; Mészáros, TH; Mészáros, TI; Mészáros, TJ; Mészáros, TK; Mészáros, TL; Mészáros, TM; Mészáros, TN; Mészáros, TO; Mészáros, TP; Mészáros, TQ; Mészáros, TR; Mészáros, TS; Mészáros, TT; Mészáros, TU; Mészáros, TV; Mészáros, TW; Mészáros, TX; Mészáros, TY; Mészáros, TZ; Mészáros, UA; Mészáros, UB; Mészáros, UC; Mészáros, UD; Mészáros, UE; Mészáros, UF; Mészáros, UG; Mészáros, UH; Mészáros, UI; Mészáros, UJ; Mészáros, UK; Mészáros, UL; Mészáros, UM; Mészáros, UN; Mészáros, UO; Mészáros, UP; Mészáros, UQ; Mészáros, UR; Mészáros, US; Mészáros, UT; Mészáros, UY; Mészáros, UZ; Mészáros, VA; Mészáros, VB; Mészáros, VC; Mészáros, VD; Mészáros, VE; Mészáros, VF; Mészáros, VG; Mészáros, VH; Mészáros, VI; Mészáros, VJ; Mészáros, VK; Mészáros, VL; Mészáros, VM; Mészáros, VN; Mészáros, VO; Mészáros, VP; Mészáros, VQ; Mészáros, VR; Mészáros, VS; Mészáros, VT; Mészáros, VU; Mészáros, VV; Mészáros, VW; Mészáros, VX; Mészáros, VY; Mészáros, VZ; Mészáros, WA; Mészáros, WB; Mészáros, WC; Mészáros, WD; Mészáros, WE; Mészáros, WF; Mészáros, WG; Mészáros, WH; Mészáros, WI; Mészáros, WJ; Mészáros, WK; Mészáros, WL; Mészáros, WM; Mészáros, WN; Mészáros, WO; Mészáros, WP; Mészáros, WQ; Mészáros, WR; Mészáros, WS; Mészáros, WT; Mészáros, WU; Mészáros, WV; Mészáros, WW; Mészáros, WX; Mészáros, WY; Mészáros, WZ; Mészáros, XA; Mészáros, XB; Mészáros, XC; Mészáros, XD; Mészáros, XE; Mészáros, XF; Mészáros, XG; Mészáros, XH; Mészáros, XI; Mészáros, XJ; Mészáros, XK; Mészáros, XL; Mészáros, XM; Mészáros, XN; Mészáros, XO; Mészáros, XP; Mészáros, XQ; Mészáros, XR; Mészáros, XS; Mészáros, XT; Mészáros, XU; Mészáros, XV; Mészáros, XW; Mészáros, XX; Mészáros, XY; Mészáros, XZ; Mészáros, YA; Mészáros, YB; Mészáros, YC; Mészáros, YD; Mészáros, YE; Mészáros, YF; Mészáros, YG; Mészáros, YH; Mészáros, YI; Mészáros, YJ; Mészáros, YK; Mészáros, YL; Mészáros, YM; Mészáros, YN; Mészáros, YO; Mészáros, YP; Mészáros, YQ; Mészáros, YR; Mészáros, YS; Mészáros, YT; Mészáros, YU; Mészáros, YV; Mészáros, YW; Mészáros, YX; Mészáros, YY; Mészáros, YZ; Mészáros, ZA; Mészáros, ZB; Mészáros, ZC; Mészáros, ZD; Mészáros, ZE; Mészáros, ZF; Mészáros, ZG; Mészáros, ZH; Mészáros, ZI; Mészáros, ZJ; Mészáros, ZK; Mészáros, ZL; Mészáros, ZM; Mészáros, ZN; Mészáros, ZO; Mészáros, ZP; Mészáros, ZQ; Mészáros, ZR; Mészáros, ZS; Mészáros, ZT; Mészáros, ZU; Mészáros, ZV; Mészáros, ZW; Mészáros, ZX; Mészáros, ZY; Mészáros, ZZ.

(Article begins on next page)



# Sensitivity of future liquid argon dark matter search experiments to core-collapse supernova neutrinos

## The DarkSide-20k Collaboration

P. Agnes<sup>1</sup> S. Albero<sup>2,3</sup> I. F. M. Albuquerque<sup>4</sup> T. Alexander<sup>5</sup> A. Alici<sup>6,7</sup> A. K. Alton<sup>8</sup>  
P. Amaudruz<sup>9</sup> S. Arcelli<sup>6,7</sup> M. Ave<sup>4</sup> I. Ch. Avetisov<sup>10</sup> R. I. Avetisov<sup>10</sup> O. Azzolini<sup>11</sup>  
H. O. Back<sup>5</sup> Z. Balmforth<sup>12</sup> V. Barbarian<sup>13</sup> A. Barrado Olmedo<sup>14</sup> P. Barrillon<sup>15</sup>  
A. Basco<sup>16</sup> G. Batignani<sup>17,18</sup> A. Bondar<sup>19,20</sup> W. M. Bonivento<sup>21</sup> E. Borisova<sup>19,20</sup>  
B. Bottino<sup>22,23</sup> M. G. Boulay<sup>24</sup> G. Buccino<sup>25</sup> S. Bussino<sup>26,27</sup> J. Busto<sup>15</sup>  
A. Buzulutskov<sup>19,20</sup> M. Cadeddu<sup>28,21</sup> M. Cadoni<sup>28,21</sup> A. Caminata<sup>23</sup> N. Canci<sup>29</sup>  
G. Cappello<sup>2,3</sup> M. Caravati<sup>21</sup> M. Cárdenas-Montes<sup>14</sup> M. Carlini<sup>30</sup> F. Carnesecchi<sup>7,31,6</sup>  
P. Castello<sup>32,21</sup> S. Catalanotti<sup>33,16</sup> V. Cataudella<sup>33,16</sup> P. Cavalcante<sup>29</sup> S. Cavuoti<sup>33,16,34</sup>  
S. Cebrian<sup>35</sup> J. M. Cela Ruiz<sup>14</sup> B. Celano<sup>16</sup> S. Chashin<sup>13</sup> A. Chepurinov<sup>13</sup> C. Cicalò<sup>21</sup>  
L. Cifarelli<sup>6,7</sup> D. Cintas<sup>35</sup> F. Coccetti<sup>31</sup> V. Cocco<sup>21</sup> M. Colocci<sup>6,7</sup> E. Conde Vilda<sup>14</sup>  
L. Consiglio<sup>29</sup> S. Copello<sup>23,22</sup> G. Covone<sup>33,16</sup> P. Czudak<sup>36</sup> S. D'Auria<sup>37</sup>  
M. D. Da Rocha Rolo<sup>38</sup> O. Dadoun<sup>39</sup> M. Daniel<sup>14</sup> S. Davini<sup>23</sup> A. De Candia<sup>33,16</sup>  
S. De Cecco<sup>40,41</sup> A. De Falco<sup>28,21</sup> G. De Filippis<sup>33,16</sup> D. De Gruttola<sup>42,43</sup> G. De Guido<sup>44</sup>  
G. De Rosa<sup>33,16</sup> M. Della Valle<sup>16,34</sup> G. Dellacasa<sup>38</sup> S. De Pasquale<sup>42,43</sup> A. V. Derbin<sup>45</sup>  
A. Devoto<sup>28,21</sup> L. Di Noto<sup>23</sup> C. Dionisi<sup>40,41</sup> G. Dolganov<sup>46</sup> F. Dordei<sup>21</sup> M. Downing<sup>47</sup>  
T. Erjavec<sup>48</sup> M. Fernandez Diaz<sup>14</sup> G. Fiorillo<sup>33,16</sup> A. Franceschi<sup>49</sup> D. Franco<sup>50</sup>  
E. Frolov<sup>19,20</sup> N. Funicello<sup>42,43</sup> F. Gabriele<sup>29</sup> C. Galbiati<sup>51,29,30</sup> M. Garbini<sup>31,7</sup>  
P. Garcia Abia<sup>14</sup> A. Gendotti<sup>52</sup> C. Ghiano<sup>29</sup> R. A. Giampaolo<sup>38,53</sup> C. Giganti<sup>39</sup>  
M. A. Giorgi<sup>18,17</sup> G. K. Giovanetti<sup>54</sup> V. Goicoechea Casanueva<sup>55</sup> A. Gola<sup>56,57</sup>  
R. Graciani Diaz<sup>58</sup> G. Y. Grigoriev<sup>46</sup> A. Grobov<sup>46,59</sup> M. Gromov<sup>13,60</sup> M. Guan<sup>61</sup>  
M. Guerzoni<sup>7</sup> M. Gulino<sup>62,63</sup> C. Guo<sup>61</sup> B. R. Hackett<sup>5</sup> A. Hallin<sup>64</sup> M. Haranczyk<sup>36</sup>  
S. Hill<sup>12</sup> S. Horikawa<sup>30,29</sup> F. Hubaut<sup>15</sup> T. Hugues<sup>65</sup> E. V. Hungerford<sup>1</sup> An. Ianni<sup>51,29</sup>  
V. Ippolito<sup>40</sup> C. C. James<sup>66</sup> C. Jillings<sup>67,68</sup> P. Kachru<sup>30,29</sup> C. L. Kendziora<sup>66</sup> G. Keppel<sup>11</sup>  
A. V. Khomyakov<sup>10</sup> S. Kim<sup>69</sup> A. Kish<sup>55</sup> I. Kochanek<sup>29</sup> K. Kondo<sup>29</sup> G. Korga<sup>12</sup>  
A. Kubankin<sup>70</sup> R. Kugathasan<sup>38,53</sup> M. Kuss<sup>17</sup> M. Kuźniak<sup>65</sup> M. La Commara<sup>71,16</sup>  
M. Lai<sup>28,21,50</sup> S. Langrock<sup>68</sup> M. Leyton<sup>16</sup> X. Li<sup>51</sup> L. Lidey<sup>5</sup> M. Lissia<sup>21</sup> G. Longo<sup>33,16</sup>  
I. N. Machulin<sup>46,59</sup> L. Mapelli<sup>51</sup> A. Marasciulli<sup>18</sup> A. Margotti<sup>7</sup> S. M. Mari<sup>26,27</sup>  
J. Maricic<sup>55</sup> M. Martínez<sup>35,72</sup> A. D. Martinez Rojas<sup>38,53</sup> C. J. Martoff<sup>69</sup> A. Masoni<sup>21</sup>  
A. Mazzi<sup>56,57</sup> A. B. McDonald<sup>73</sup> J. Mclaughlin<sup>9,12</sup> A. Messina<sup>40,41</sup> P. D. Meyers<sup>51</sup>  
T. Miletic<sup>55</sup> R. Milincic<sup>55</sup> A. Moggi<sup>17</sup> A. Moharana<sup>30,29</sup> S. Moiola<sup>44</sup> J. Monroe<sup>12</sup>  
S. Morisi<sup>33,16</sup> M. Morrocchi<sup>17,18</sup> E. N. Mozhevitina<sup>10</sup> T. Mróz<sup>36</sup> V. N. Muratova<sup>45</sup>  
C. Muscas<sup>32,21</sup> L. Musenich<sup>23,22</sup> P. Musico<sup>23</sup> R. Nania<sup>7</sup> T. Napolitano<sup>49</sup>  
A. Navrer Agasson<sup>39</sup> M. Nessi<sup>25</sup> I. Nikulin<sup>70</sup> J. Nowak<sup>74</sup> A. Oleinik<sup>70</sup> V. Oleynikov<sup>19,20</sup>  
L. Pagani<sup>48</sup> M. Pallavicini<sup>22,23</sup> L. Pandola<sup>63</sup> E. Pantic<sup>48</sup> E. Paoloni<sup>17,18</sup>  
G. Paternoster<sup>56,57</sup> P. A. Pegoraro<sup>32,21</sup> L. A. Pellegrini<sup>44</sup> C. Pellegrino<sup>7,31</sup> F. Perotti<sup>75,37</sup>  
V. Pesudo<sup>14</sup> E. Picciau<sup>28,21</sup> F. Pietropaolo<sup>25</sup> A. Pocar<sup>47</sup> D. M. Poehlmann<sup>48</sup> S. Pordes<sup>66</sup>  
S. S. Poudel<sup>1</sup> P. Pralavorio<sup>15</sup> D. Price<sup>76</sup> F. Raffaelli<sup>17</sup> F. Ragusa<sup>77,37</sup> A. Ramirez<sup>1</sup>  
M. Razeti<sup>21</sup> A. Razeto<sup>29</sup> A. L. Renshaw<sup>1</sup> S. Rescia<sup>78</sup> M. Rescigno<sup>40</sup> F. Resnati<sup>25</sup>

**F. Retiere**<sup>9</sup> **L. P. Rignanese**<sup>7,6</sup> **C. Ripoli**<sup>43,42</sup> **A. Rivetti**<sup>38</sup> **J. Rode**<sup>39,50</sup> **L. Romero**<sup>14</sup>  
**M. Rossi**<sup>23,22</sup> **A. Rubbia**<sup>52</sup> **P. Salatino**<sup>79,16</sup> **O. Samoylov**<sup>60</sup> **E. Sánchez García**<sup>14</sup>  
**E. Sandford**<sup>76</sup> **S. Sanfilippo**<sup>27,26</sup> **D. Santone**<sup>12</sup> **R. Santorelli**<sup>14</sup> **C. Savarese**<sup>51</sup>  
**E. Scapparone**<sup>7</sup> **B. Schlitzer**<sup>48</sup> **G. Scioli**<sup>6,7</sup> **D. A. Semenov**<sup>45</sup> **B. Shaw**<sup>9</sup> **A. Shchagin**<sup>70</sup>  
**A. Sheshukov**<sup>60</sup> **M. Simeone**<sup>79,16</sup> **P. Skensved**<sup>73</sup> **M. D. Skorokhvatov**<sup>46,59</sup> **O. Smirnov**<sup>60</sup>  
**B. Smith**<sup>9</sup> **A. Sokolov**<sup>19,20</sup> **A. Steri**<sup>21</sup> **S. Stracka**<sup>17</sup> **V. Strickland**<sup>24</sup> **M. Stringer**<sup>73</sup>  
**S. Sulis**<sup>32,21</sup> **Y. Suvorov**<sup>33,16,46</sup> **A. Szec**<sup>76</sup> **R. Tartaglia**<sup>29</sup> **G. Testera**<sup>23</sup> **T. N. Thorpe**<sup>30,29</sup>  
**A. Tonazzo**<sup>50</sup> **S. Torres-Lara**<sup>1</sup> **A. Tricomi**<sup>2,3</sup> **E. V. Unzhakov**<sup>45</sup> **G. Usai**<sup>28,21</sup>  
**T. Vallivilayil John**<sup>30,29</sup> **T. Viant**<sup>52</sup> **S. Viel**<sup>24</sup> **A. Vishneva**<sup>60</sup> **B. Vogelaar**<sup>80</sup> **M. Wada**<sup>65</sup>  
**H. Wang**<sup>81</sup> **Y. Wang**<sup>81</sup> **S. Westerdale**<sup>21</sup> **R. J. Wheadon**<sup>38</sup> **L. Williams**<sup>82</sup> **Ma. M. Wojcik**<sup>36</sup>  
**Ma. Wojcik**<sup>83</sup> **X. Xiao**<sup>81</sup> **C. Yang**<sup>61</sup> **A. Zani**<sup>25</sup> **A. Zichichi**<sup>6,7</sup> **M. Ziembicki**<sup>65</sup> **G. Zuzel**<sup>36</sup>  
**M. P. Zykova**<sup>10</sup>

<sup>1</sup>Department of Physics, University of Houston, Houston, TX 77204, USA

<sup>2</sup>INFN Catania, Catania 95121, Italy

<sup>3</sup>Università of Catania, Catania 95124, Italy

<sup>4</sup>Instituto de Física, Universidade de São Paulo, São Paulo 05508-090, Brazil

<sup>5</sup>Pacific Northwest National Laboratory, Richland, WA 99352, USA

<sup>6</sup>Physics Department, Università degli Studi di Bologna, Bologna 40126, Italy

<sup>7</sup>INFN Bologna, Bologna 40126, Italy

<sup>8</sup>Physics Department, Augustana University, Sioux Falls, SD 57197, USA

<sup>9</sup>TRIUMF, 4004 Wesbrook Mall, Vancouver, BC V6T 2A3, Canada

<sup>10</sup>Mendeleev University of Chemical Technology, Moscow 125047, Russia

<sup>11</sup>INFN Laboratori Nazionali di Legnaro, Legnaro (Padova) 35020, Italy

<sup>12</sup>Department of Physics, Royal Holloway University of London, Egham TW20 0EX, UK

<sup>13</sup>Skobeltsyn Institute of Nuclear Physics, Lomonosov Moscow State University, Moscow 119234, Russia

<sup>14</sup>CIEMAT, Centro de Investigaciones Energéticas, Medioambientales y Tecnológicas, Madrid 28040, Spain

<sup>15</sup>Centre de Physique des Particules de Marseille, Aix Marseille Univ, CNRS/IN2P3, CPPM, Marseille, France

<sup>16</sup>INFN Napoli, Napoli 80126, Italy

<sup>17</sup>INFN Pisa, Pisa 56127, Italy

<sup>18</sup>Physics Department, Università degli Studi di Pisa, Pisa 56127, Italy

<sup>19</sup>Budker Institute of Nuclear Physics, Novosibirsk 630090, Russia

<sup>20</sup>Novosibirsk State University, Novosibirsk 630090, Russia

<sup>21</sup>INFN Cagliari, Cagliari 09042, Italy

<sup>22</sup>Physics Department, Università degli Studi di Genova, Genova 16146, Italy

<sup>23</sup>INFN Genova, Genova 16146, Italy

<sup>24</sup>Department of Physics, Carleton University, Ottawa, ON K1S 5B6, Canada

<sup>25</sup>CERN, European Organization for Nuclear Research 1211 Geneve 23, Switzerland, CERN

<sup>26</sup>INFN Roma Tre, Roma 00146, Italy

<sup>27</sup>Mathematics and Physics Department, Università degli Studi Roma Tre, Roma 00146, Italy

<sup>28</sup>Physics Department, Università degli Studi di Cagliari, Cagliari 09042, Italy

<sup>29</sup>INFN Laboratori Nazionali del Gran Sasso, Assergi (AQ) 67100, Italy

<sup>30</sup>Gran Sasso Science Institute, L'Aquila 67100, Italy

- <sup>31</sup>Museo della fisica e Centro studi e Ricerche Enrico Fermi, Roma 00184, Italy
- <sup>32</sup>Department of Electrical and Electronic Engineering, Università degli Studi di Cagliari, Cagliari 09123, Italy
- <sup>33</sup>Physics Department, Università degli Studi “Federico II” di Napoli, Napoli 80126, Italy
- <sup>34</sup>INAF Osservatorio Astronomico di Capodimonte, 80131 Napoli, Italy
- <sup>35</sup>Centro de Astropartículas y Física de Altas Energías, Universidad de Zaragoza, Zaragoza 50009, Spain
- <sup>36</sup>M. Smoluchowski Institute of Physics, Jagiellonian University, 30-348 Krakow, Poland
- <sup>37</sup>INFN Milano, Milano 20133, Italy
- <sup>38</sup>INFN Torino, Torino 10125, Italy
- <sup>39</sup>LPNHE, CNRS/IN2P3, Sorbonne Université, Université Paris Diderot, Paris 75252, France
- <sup>40</sup>INFN Sezione di Roma, Roma 00185, Italy
- <sup>41</sup>Physics Department, Sapienza Università di Roma, Roma 00185, Italy
- <sup>42</sup>Physics Department, Università degli Studi di Salerno, Salerno 84084, Italy
- <sup>43</sup>INFN Salerno, Salerno 84084, Italy
- <sup>44</sup>Chemistry, Materials and Chemical Engineering Department “G. Natta”, Politecnico di Milano, Milano 20133, Italy
- <sup>45</sup>Saint Petersburg Nuclear Physics Institute, Gatchina 188350, Russia
- <sup>46</sup>National Research Centre Kurchatov Institute, Moscow 123182, Russia
- <sup>47</sup>Amherst Center for Fundamental Interactions and Physics Department, University of Massachusetts, Amherst, MA 01003, USA
- <sup>48</sup>Department of Physics, University of California, Davis, CA 95616, USA
- <sup>49</sup>INFN Laboratori Nazionali di Frascati, Frascati 00044, Italy
- <sup>50</sup>APC, Université de Paris, CNRS, Astroparticule et Cosmologie, Paris F-75013, France
- <sup>51</sup>Physics Department, Princeton University, Princeton, NJ 08544, USA
- <sup>52</sup>Institute for Particle Physics, ETH Zürich, Zürich 8093, Switzerland
- <sup>53</sup>Department of Electronics and Communications, Politecnico di Torino, Torino 10129, Italy
- <sup>54</sup>Williams College, Physics Department, Williamstown, MA 01267 USA
- <sup>55</sup>Department of Physics and Astronomy, University of Hawai’i, Honolulu, HI 96822, USA
- <sup>56</sup>Fondazione Bruno Kessler, Povo 38123, Italy
- <sup>57</sup>Trento Institute for Fundamental Physics and Applications, Povo 38123, Italy
- <sup>58</sup>Universitat de Barcelona, Barcelona E-08028, Catalonia, Spain
- <sup>59</sup>National Research Nuclear University MEPhI, Moscow 115409, Russia
- <sup>60</sup>Joint Institute for Nuclear Research, Dubna 141980, Russia
- <sup>61</sup>Institute of High Energy Physics, Beijing 100049, China
- <sup>62</sup>Engineering and Architecture Faculty, Università di Enna Kore, Enna 94100, Italy
- <sup>63</sup>INFN Laboratori Nazionali del Sud, Catania 95123, Italy
- <sup>64</sup>Department of Physics, University of Alberta, Edmonton, AB T6G 2R3, Canada
- <sup>65</sup>AstroCeNT, Nicolaus Copernicus Astronomical Center of the Polish Academy of Sciences, 00-614 Warsaw, Poland
- <sup>66</sup>Fermi National Accelerator Laboratory, Batavia, IL 60510, USA
- <sup>67</sup>SNOLAB, Lively, ON P3Y 1N2, Canada
- <sup>68</sup>Department of Physics and Astronomy, Laurentian University, Sudbury, ON P3E 2C6, Canada

- <sup>69</sup>Physics Department, Temple University, Philadelphia, PA 19122, USA
- <sup>70</sup>Radiation Physics Laboratory, Belgorod National Research University, Belgorod 308007, Russia
- <sup>71</sup>Pharmacy Department, Università degli Studi “Federico II” di Napoli, Napoli 80131, Italy
- <sup>72</sup>Fundación ARAID, Universidad de Zaragoza, Zaragoza 50009, Spain
- <sup>73</sup>Department of Physics, Engineering Physics and Astronomy, Queen’s University, Kingston, ON K7L 3N6, Canada
- <sup>74</sup>Physics Department, Lancaster University, Lancaster LA1 4YB, UK
- <sup>75</sup>Civil and Environmental Engineering Department, Politecnico di Milano, Milano 20133, Italy
- <sup>76</sup>Department of Physics and Astronomy, The University of Manchester, Manchester M13 9PL, UK
- <sup>77</sup>Physics Department, Università degli Studi di Milano, Milano 20133, Italy
- <sup>78</sup>Brookhaven National Laboratory, Upton, NY 11973, USA
- <sup>79</sup>Chemical, Materials, and Industrial Production Engineering Department, Università degli Studi “Federico II” di Napoli, Napoli 80126, Italy
- <sup>80</sup>Virginia Tech, Blacksburg, VA 24061, USA
- <sup>81</sup>Physics and Astronomy Department, University of California, Los Angeles, CA 90095, USA
- <sup>82</sup>Department of Physics and Engineering, Fort Lewis College, Durango, CO 81301, USA
- <sup>83</sup>Institute of Applied Radiation Chemistry, Lodz University of Technology, 93-590 Lodz, Poland

**Abstract.** Future liquid-argon DarkSide-20k and Argo detectors, designed for direct dark matter search, will be sensitive also to core-collapse supernova neutrinos, via coherent elastic neutrino-nucleus scattering. This interaction channel is flavor-insensitive with a high-cross section, enabling for a high-statistics neutrino detection with target masses of  $\sim 50$  t and  $\sim 360$  t for DarkSide-20k and Argo respectively.

Thanks to the low-energy threshold of  $\sim 0.5$  keV<sub>nr</sub> achievable by exploiting the ionization channel, DarkSide-20k and Argo have the potential to discover supernova bursts throughout our galaxy and up to the Small Magellanic Cloud, respectively, assuming a  $11-M_{\odot}$  progenitor star. We report also on the sensitivity to the neutronization burst, whose electron neutrino flux is suppressed by oscillations when detected via charged current and elastic scattering. Finally, the accuracies in the reconstruction of the average and total neutrino energy in the different phases of the supernova burst, as well as its time profile, are also discussed, taking into account the expected background and the detector response.

**Keywords:** supernova neutrinos, core-collapse supernovae, dark matter detectors, coherent elastic neutrino nucleus scattering

---

## Contents

<b>1</b>	<b>Introduction</b>	<b>1</b>
<b>2</b>	<b>Core-collapse supernovae and neutrinos</b>	<b>2</b>
<b>3</b>	<b>Supernova neutrino signal and detector response</b>	<b>3</b>
<b>4</b>	<b>Expected background in GADMC TPCs</b>	<b>6</b>
<b>5</b>	<b>Sensitivity to supernova neutrinos</b>	<b>9</b>
<b>6</b>	<b>Conclusions</b>	<b>13</b>

---

## 1 Introduction

Core-collapse supernovae (SNe) are violent explosions of very massive stars at the end of their lives, triggered by the gravitational collapse of the stellar cores [1]. The characteristic energy emitted by a core-collapse SN is  $\sim 10^{53}$  erg, which corresponds to the gravitational binding energy of a  $1.4 M_{\odot}$  core that collapses into a neutron star. 99% of this energy is emitted as neutrinos,  $\sim 1\%$  goes into the kinetic energy associated with the external layers of the progenitor that are ejected at  $\sim 10,000$  km/s, and only 0.01% is radiated at UV, optical and near-infrared wavelengths. Therefore neutrinos are the ideal “messengers” for investigating the final stages of stellar evolution, even when the SN is not accessible to optical and radio telescopes [2–5]. Observations of a neutrino burst from SN 1987A have suggested that the formation of a neutron star might have occurred inside the SN remnant, nevertheless, this fact has been never unambiguously confirmed. SN can play also a key role in the neutrino physics, by providing constraints to the neutrino absolute mass and mass ordering [6, 7].

To date, the only SN observed through neutrinos is the SN 1987A, with a total of 25 events detected by Kamiokande-2 [2], IMB [3] and Baksan [4]. Since then, core-collapse SN simulations have made several breakthroughs, providing detailed understanding of the neutronization, accretion, and cooling phases [5, 7]. The next detection of galactic SN neutrinos will provide key elements to our comprehension of the mechanisms governing the core-collapse and also on fundamental questions in neutrino physics.

This paper presents a sensitivity study on SN neutrino detection with the Global Argon Dark Matter Collaboration (GADMC) liquid-argon (LAr) experiments, DarkSide-20k and Argo. DarkSide-20k is a dual-phase time-projection-chamber (TPC) of about 50 t mass [8], designed for dark matter detection, but also sensitive to low energy nuclear recoils (NR) induced by SN neutrinos via coherent elastic neutrino-nucleus scattering ( $\text{CE}\nu\text{NS}$ ) [9], in construction at Laboratori Nazionali del Gran Sasso LNGS), Italy. The GADMC is also considering a future single-phase or dual-phase multi-hundred tonne detector, called Argo, with SNOLAB, Canada, as the preferred location. For this work we assume that Argo is a dual-phase TPC with a target mass of 370 t.

Neutrino detection via  $\text{CE}\nu\text{NS}$  offers a unique opportunity, since it is equally sensitive to all neutrino flavours and therefore allows to measure the unoscillated SN neutrino flux. Current and future giant (kilotons and megatons target mass) detectors, in fact, are

mostly sensitive to electron neutrinos: water-Cherenkov detectors like Super-Kamiokande [10], Hyper-Kamiokande [11], IceCube [12], and KM3NeT [13] rely on the inverse beta decay (IBD) channel; the DUNE [14] LAr TPC will exploit the  $\nu_e {}^{40}\text{Ar} \rightarrow {}^{40}\text{K}^* e^-$  charge current interaction; scintillator detectors like JUNO [15] will look at IBD and elastic scattering channels.

An additional advantage of the  $\text{CE}\nu\text{NS}$  channel is the high cross-section, roughly 50 times larger than that of charge current interaction [16] at 10 MeV, which compensates for the relatively small target masses of DarkSide-20k and Argo, and which allows for high-statistics detections.

The sensitivity to SN neutrino detection via  $\text{CE}\nu\text{NS}$  process has been thoroughly investigated for future liquid xenon dark matter detectors like XENONnT, DARWIN, and LZ [17, 18]. Although the lower LAr density imposes larger TPC volumes with respect to liquid xenon experiments, and hence a slightly worse time resolution due to the longer drift time, LAr experiments can provide a better energy resolution. The lighter argon nucleus and the smaller energy quenching effect, in fact, as demonstrated in this work, provide higher sensitivity to SN burst parameters that can be inferred from the nuclear recoil energy spectrum induced by SN neutrinos. In addition, the lower energy threshold allows for larger statistics, compensating for the lower cross-section with respect to liquid xenon targets.

In this work, we provide an extensive study for argon detectors, assuming a background level derived from the most recent contamination measurements from material screenings. After a detailed description of the expected signal (section 2), of the detector response (section 3) and of the expected background (section 4), we discuss the DarkSide-20k and Argo discovery potential to SN burst in section 5. We will also report on the sensitivity to the neutronization burst and to the mean and integrated neutrino energies from the SN accretion and cooling phases.

## 2 Core-collapse supernovae and neutrinos

A very massive star can undergo core-collapse when, at the end of its life, the iron core of the progenitor star, grows to roughly the Chandrasekhar mass, and nuclear fusion can no longer balance the inward push from the force of gravity. In this regime, neutrinos are mostly produced by electron captures on heavy nuclei and leave the core unimpeded. After a few milliseconds, the neutrino mean free path becomes comparable to the core radius and neutrinos remain trapped in ultra-dense matter. [19]. Despite the trapping, neutrinos around the newly formed neutrinosphere can still escape.

When compression of matter reaches a critical density, the core rebounds. The violent rebound of the matter produces a pressure wave propagating outwards, which eventually steepens into a shock wave, and neutrino emission again increases rapidly, producing the so-called neutronization burst, lasting about 30 ms. The shock, in fact, is so powerful that it dissociates nuclei into free nucleons all along its way to the edge of the core. Free protons quickly interact with the energetic electrons, resulting in neutrons and electron neutrinos. [20, 21].

Neutrinos are the only messengers that can bring us direct information about the neutronization phase. During their propagation through the stellar mantle to Earth, neutrinos oscillate, with a flavor conversion amplified by the Mikheev-Smirnov-Wolfenstein (MSW) effect [22], in agreement with the matter density profile crossed. Additional phenomena, such as matter turbulence, fluctuations in stellar matter density, and neutrino-neutrino interactions,



can lead to alteration of the MSW effect, and hence of neutrino flavor conversion. As a net effect, the survival probability at the Earth of  $\nu_e$ 's, produced in the neutronization phase, is expected to be  $\sim 2\%$  ( $\sim 30\%$ ) assuming the normal (inverted) mass ordering [6, 23, 24].

This electronic flavor suppression, together with the low statistics, did not allow the neutronization burst to be observed in SN1987A. Even future experiments, primarily relying on charge current interactions, will be significantly limited in their sensitivity to the neutronization burst. In contrast, neutrino flavor conversion does not affect the results reported in this work, as CE $\nu$ NS is flavor insensitive, and therefore GADMC LAr TPCs will be able to detect the entire SN neutrino flux. Furthermore, it is interesting to observe how the comparison of the interaction rates measured by these TPCs with the future charge current measurements, mentioned in the previous section, will allow improving constraints on the neutrino mass ordering.

After the neutronization, the shock wave may stall losing energy in the dissociation of the nuclei, thus being unable to overcome the ram pressure of the material falling into the shock. Neutrinos can revitalize the shock, depositing energy into the envelope. This critical stage, named accretion phase, lasts a few hundred milliseconds and can lead either to the star explosion or to its collapse, and thus to the formation of a black hole. Multi-dimensional simulations suggest a standing accretion shock instability (SASI) [25], where the shock front oscillates inward and outward, periodically, leading to a  $\mathcal{O}(10 - 100)$  Hz modulation of the neutrino luminosity. Although this effect can potentially be observed with GADMC TPCs, thanks to the time resolution in the millisecond range, the present work is based on 1D simulations, and therefore sensitivity to SASI will not be discussed.

The explosion of the SN blows off almost all the matter in the stellar mantle and leaves the hot proto-neutron star. The third phase, the cooling of the neutron star by neutrino emission, lasts about 10 s [20]. The neutrino mean energy  $\langle E_\nu \rangle$  drops from 15 MeV to 5 MeV in about 10 s, while the neutrino luminosity decreases roughly according to the law of black body radiation [26].

The luminosity and mean energy time evolutions and the energy spectrum are shown in figure 1 from hydrodynamical spherically symmetric core-collapse SN simulations by the Garching group [7, 27, 28], for a progenitor star mass of  $27 M_\odot$ . This is the reference model adopted in this work, and we will report results also for a progenitor star mass of  $11 M_\odot$ .

### 3 Supernova neutrino signal and detector response

The CE $\nu$ NS differential cross-section as a function of neutrino energy,  $E_\nu$ , and recoil energy,  $E_r$ , is given by

$$d\sigma(E_\nu, E_r) = \frac{G_F^2}{4\pi} Q_W^2 m \left( 1 - \frac{mE_r}{2E_\nu^2} \right) F^2(q) dE_r, \quad (3.1)$$

where  $G_F$  is the Fermi coupling constant,  $Q_W$  the weak charge of argon nucleus, and  $m$  the argon nucleus mass.  $F(q)$  is the Helm form factor, parametrized with the Lewin-Smith approach [29], as a function of the momentum transfer  $q = \sqrt{2mE_r}$ .

The nuclear recoil (NR) energy spectrum induced by SN neutrinos, shown in figure 2, results from the convolution of the neutrino flux with the differential neutrino cross-section from eq. 3.1. The window of observation is  $<100$  keV $_{nr}$ , with  $\sim 70\%$  ( $\sim 50\%$ ) of events with energy  $<10$  keV $_{nr}$  ( $<5$  keV $_{nr}$ ). The low energy detection threshold, therefore, plays a crucial role in the final sensitivity.

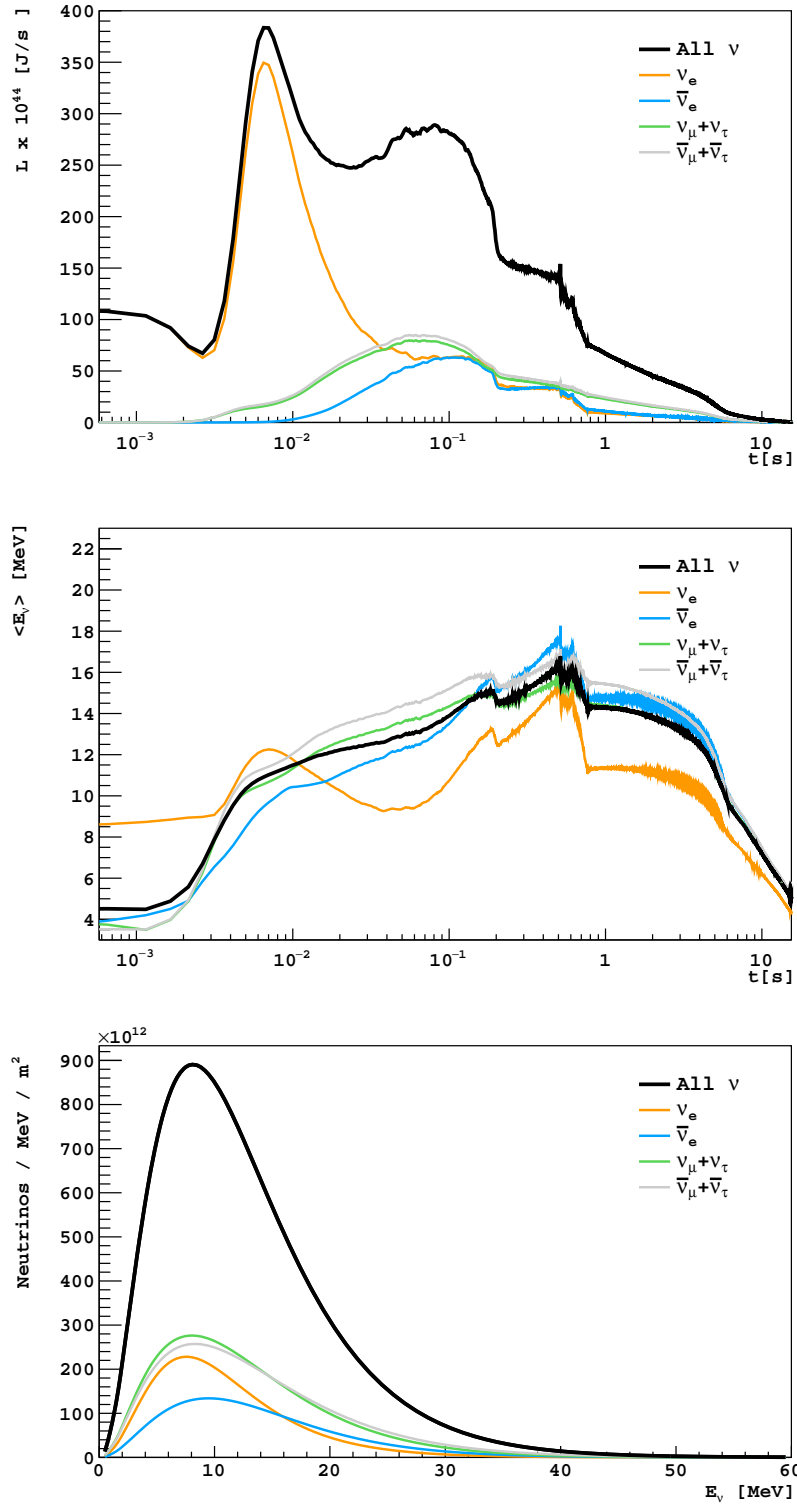


**Figure 1.** Time evolutions of neutrino luminosity (top) and mean energy (middle) and energy spectrum (bottom) from a core-collapse  $27 M_{\odot}$  SN for the different neutrino species, using Garching group 1-d simulations [20].

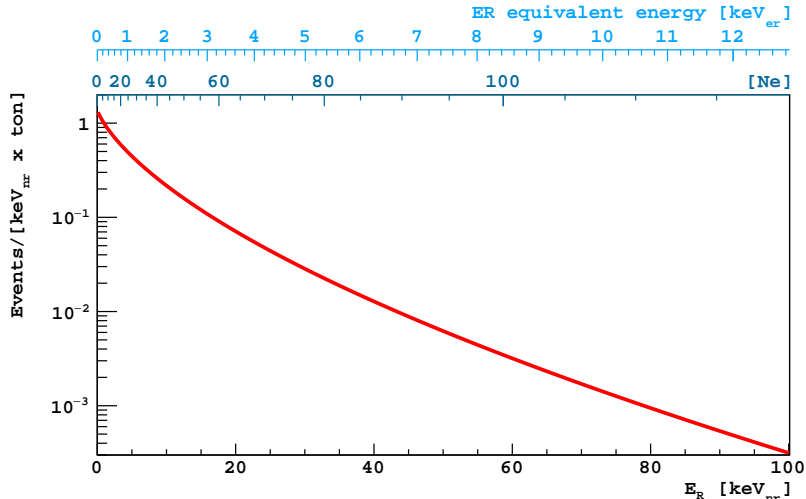


**Figure 2.** Nuclear recoil energy spectrum from neutrino interactions in LAr via  $\text{CE}\nu\text{NS}$  from a core-collapse  $27 M_{\odot}$  supernova at 10 kpc.

The detection mechanism of interacting particles in dual-phase GADMC LAr TPCs relies on a prompt light pulse (S1) induced by scintillation, followed by a delayed pulse (S2) associated to ionization electrons. These, in fact, are drifted vertically upwards by the drift field, and extracted, by the so-called extraction field, in a thin layer of gas, where they induce a secondary light signal by electroluminescence.

The detection efficiency of S1 photons is estimated in DarkSide-20k at 19% through Monte Carlo simulations. Therefore, a detection strategy based on S1 photons trigger, highly inefficient for NRs in the  $\text{keV}_{nr}$  range, would strongly affect the sensitivity to SN neutrinos. Disregarding S1, S2 guarantees an amplification factor by more than 20 ( $\sim 23$  photoelectrons per electron extracted in the gaseous phase in DarkSide-50 [30]), allowing the detection of NRs with a threshold of a few hundreds of  $\text{eV}_{nr}$ . This approach was successfully applied by DarkSide-50 in setting the world’s best limit on WIMP dark matter particles in the 2-6  $\text{GeV}/c^2$  mass range [30], with a  $\sim 0.6 \text{ keV}_{nr}$  threshold. In the same work, DarkSide-50 demonstrated a detection efficiency at 100% level for NR deposits with an energy of  $0.46 \text{ keV}_{nr}$ , allowing the detection of about 86% of NRs induced by SN neutrinos.

The dual-phase LAr TPC response to NRs, in the S2 channel, differs from the one to electronic recoils (ERs), which account for almost all of the background. This is due to the differences between ER and NR excitons to ionization electrons ratio, as well as to the recombination process, which produces excited argon dimers and depletes the ionization channel. In addition, the largest fraction of energy deposited by NRs is neither converted into scintillation nor ionization, resulting in a quenching effect much stronger than that observable for ERs [31].

The NR energy scale in the S2 observable was determined with  $^{241}\text{Am}-^9\text{Be}$  and  $^{241}\text{Am}-^{13}\text{C}$  neutron sources [30] deployed outside the DarkSide-50 cryostat, and from neutron-beam scattering data from the SCENE [32] and ARIS [31] experiments. The S2 ER energy scale is obtained from DarkSide-50 data by fitting the Thomas-Imel model [33] to the mean S2 measured for the 2.82 keV K-shell and 0.27 keV L-shell lines from the electron capture of the cosmogenic  $^{37}\text{Ar}$  [34]. At the nominal drift field of 200 V/cm at which GADMC TPCs operate, and using S2 as energy variable, the ER energy corresponding to 100  $\text{keV}_{nr}$  is about 13  $\text{keV}_{er}$ , as shown in figure 2.

The energy resolution model adopted in this work accounts for the LAr intrinsic fluctuations of the ionization and electron-ion recombination processes, and for the statistics governing the emission and detection of photons induced by electrons in the gas pocket. Intrinsic processes fluctuate with respect to the binomial probability defined as the ratio of the number of free ionization electrons and the number of all quanta produced by the particle interaction. The latter is obtained by dividing the deposited energy by the effective work function in LAr (19.5 eV [35]). The photoelectron statistics is assumed normal, with a photon yield of 23 photoelectrons per ionization electron, in agreement with the DarkSide-50 measurement.

The event time resolution is dominated by the electron drift time, which, in absence of a S1 pulse, induces a delay with respect to the SN neutrino interaction time. The drift velocity in presence of an electric field of 200 V/cm is  $(0.93 \pm 0.01)$  mm/ $\mu$ s, which corresponds to a maximum drift time,  $T_{max}$  of  $\sim 3.8$  ms in DarkSide-20k (3.5 m height), and of  $\sim 5.4$  ms in Argo (5.0 m height). As SN neutrino events are uniformly distributed in the TPC, the corresponding standard deviations, calculated as  $T_{max}/\sqrt{12}$ , are  $\sim 1.1$  ms and  $\sim 1.6$  ms, respectively.

The same response model is applied to energy deposits from the background sources discussed in the next section.

#### 4 Expected background in GADMC TPCs

The DarkSide-20k (Argo) TPC is an octagonal regular prism with a distance of 3.5 m (8 m) between parallel lateral walls, resulting in a total active LAr mass of 49.7 t (371 t). Differently from DarkSide-50, where the TPC is housed in a stainless steel cryostat, DarkSide-20k and Argo TPCs will be enclosed in an acrylic envelope, characterized by a larger radio-purity and smaller mass. This will be possible thanks to the new design, where the TPC is entirely immersed in a LAr bath within a proto-DUNE-like cryostat, serving as active and passive shielding against cosmic rays and environmental radioactivity, respectively. In this new design, photomultiplier tubes that detect light in DarkSide-50 will be replaced by silicon photomultipliers (SiPMs), which provide higher quantum efficiency and radiopurity [8, 36].

The background expected in the energy range of observation for SN neutrinos ( $< 100$  keV $_{nr}$ ) can be inferred from the one measured in DarkSide-50. Above  $\sim 1$  keV $_{nr}$ , this is dominated by LAr intrinsic contamination from  $^{39}\text{Ar}$  and  $^{85}\text{Kr}$   $\beta$ -decays, and by radioactivity from the detector materials surrounding the active mass.

$^{39}\text{Ar}$  has a cosmogenic origin, as it is produced by cosmic rays via spallation on  $^{40}\text{Ar}$ . In order to suppress such a background, the LAr active mass is extracted from deep underground wells (UAr) in Cortez, Colorado (USA), naturally shielded against cosmic rays. DarkSide-50 has measured an  $^{39}\text{Ar}$  specific activity of  $\sim 0.7$  mBq/kg. In the same campaign,  $^{85}\text{Kr}$  was identified with a specific activity of  $\sim 2$  mBq/kg. The anthropogenic nature of  $^{85}\text{Kr}$  suggests tiny air contamination in UAr occurred during the detector filling, possibly at the origin also of the residual  $^{39}\text{Ar}$  activity. This hypothesis, corroborated later by the identification of a leak in the purification phase, suggests an even smaller  $^{39}\text{Ar}$  intrinsic contamination in UAr. For both DarkSide-20k and Argo, any residual  $^{85}\text{Kr}$  activity will be entirely suppressed by distillation thanks to Aria, a 350 m tall distillation column in the phase of installation in the Seruci mine in Sardinia [8]. In this work,  $^{85}\text{Kr}$  contamination is therefore assumed negligible, but we consider the most conservative hypothesis on  $^{39}\text{Ar}$  specific activity, corresponding to the one measured by DarkSide-50 in UAr. As shown in figure 3 (top) that displays the

energy distribution of expected signal and background, the contribution from  $^{39}\text{Ar}$  becomes comparable to the signal from a 10 kpc 11- $M_{\odot}$  SN at  $\sim 100$  number of ionization electrons,  $N_{e^-}$ , corresponding to  $\sim 8.5$  keV $_{er}$ . The total expected rate of  $^{39}\text{Ar}$  events in DarkSide-20k (Argo) is 0.5 Hz (4.2 Hz), taking into account that the fraction of  $^{39}\text{Ar}$  events with  $N_{e^-} < 100$  is  $\sim 1.7\%$ .

The external background rate is estimated from the contamination, measured in material screening campaigns (not yet completed at the time of writing), of radioactive chains ( $^{238}\text{U}$ ,  $^{235}\text{U}$  and  $^{232}\text{Th}$ ) and individual isotopes ( $^{137}\text{Cs}$ ,  $^{53}\text{Mn}$ ,  $^{40}\text{K}$ ,  $^{60}\text{Co}$ ). Each contaminant was simulated with G4DS [35], the DarkSide Monte Carlo package, tracking the radiation from the detector components, primarily from the acrylic vessel and SiPMs. Since SN neutrinos interact only once in LAr, multiple-scatter events, identified by the detection of multiple S2 pulses, are efficiently rejected. The rate of the residual single-scatter events in DarkSide-20k (Argo) is expected to be  $\sim 75$  Hz ( $\sim 320$  Hz) in the entire energy range. Narrowing in the region of interest for SN neutrinos, the rate drops to  $\sim 0.3$  Hz ( $\sim 1.3$  Hz).

Simulations demonstrate that the mean attenuation length in LAr of single-scatter ER events from the external background, with energy less than  $< 8.5$  keV $_{er}$ , is  $\sim 0.5$  cm. The external contamination becomes thus negligible by rejecting events within 5 cm from the detector walls. The event position is reconstructed at the centimeter level on the plane orthogonal to the electric field, exploiting the S2 signal and the segmentation of the photodetection modules. The active mass resulting from the volume fiducialization is 47.1 t in DarkSide-20k and 362.7 t in Argo.

The events originating from the upper and lower planes can be ideally suppressed using the dependence of the ionization electron cloud diffusion on the vertical position, as discussed in [37]. However, since we don't have an estimate of the rejection efficiency at such low energies, the background from the top and bottom planes is conservatively included in this study. Its residual rate is 0.2 Hz in DarkSide-20k and 1.1 Hz in Argo.

The sub-keV $_{nr}$  energy region is dominated by a large population of spurious electrons, here named "single-electrons", whose origin is still under investigation. A fraction of these events is related to impurities present in LAr that capture drift electrons and re-emit them with a delay that varies from a few milliseconds to several seconds. A time correlation has been observed in DarkSide-50 between a fraction of single-electrons and events with an large amplitude S2 pulse preceding them. However, the mechanism behind the majority of single electrons remains unknown.

In this work, we assume, for the single-electron background, the spectrum of single-electrons as measured in DarkSide-50, after subtraction of known internal and external background components [30], scaling the rate by the target mass ratio between DarkSide-50 and DarkSide-20k or Argo. The single electron rate measured in DarkSide-50 is  $\sim 380$  mHz/ton, and drops to  $\sim 1.8$  mHz/ton by applying a threshold cut at  $N_{e^-} \geq 3$ , as shown in figure 3 for neutrino signals from 11- $M_{\odot}$  and 27- $M_{\odot}$  SNe. Pile-up of single electrons with physics events are expected with probabilities equal to 6% and 49% for DarkSide-20k and Argo, respectively. The single electron component in such events can be efficiently identified and removed by applying selection cuts on the spatial distance between the two interactions.

The window of observation is then defined within 8 s from the burst and between 3 and 100  $N_{e^-}$ , in order to suppress single-electron background and  $^{39}\text{Ar}$  events, respectively. The neutrino detection efficiency via CE $\nu$ NS in the [3, 100]  $N_{e^-}$  range, shown in figure 4, leads to expected number of signal events in DarkSide-20k (Argo) of 181.4 (1396.6) and 336.5 (2591.6) from 11- $M_{\odot}$  and 27- $M_{\odot}$  SN burst at 10 kpc, as quoted in table 1.

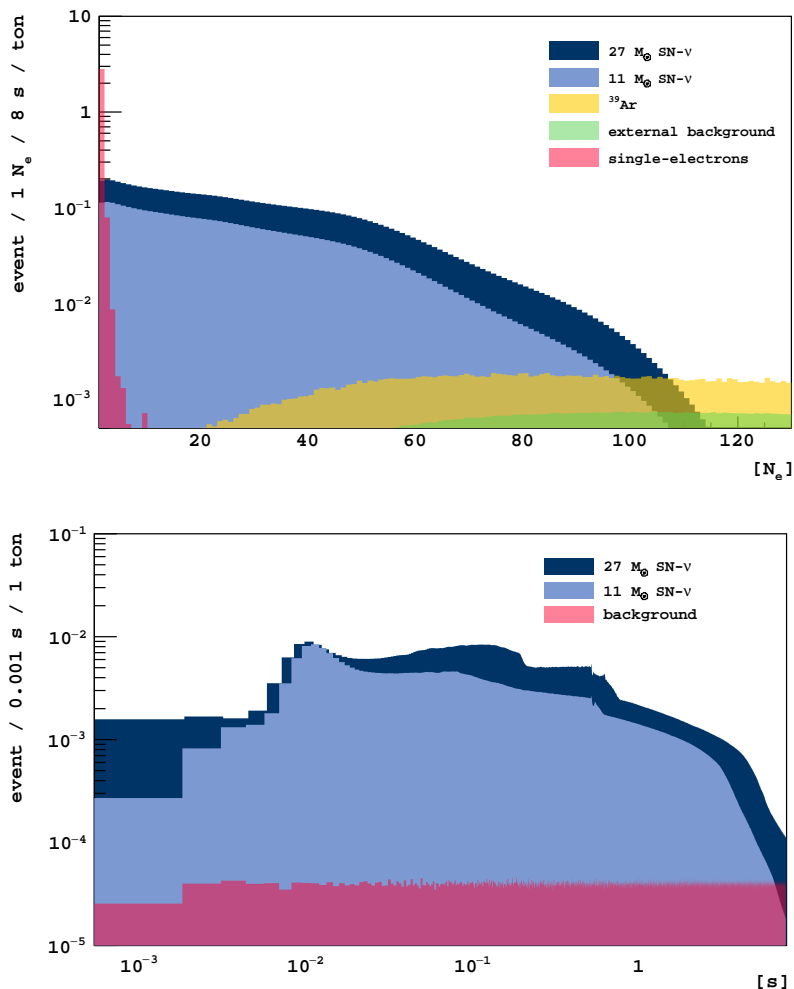


**Figure 3.** Top. Energy spectrum in number of ionization electrons ( $N_{e^-}$ ) per unit of mass of neutrinos from  $11 M_{\odot}$  and  $27 M_{\odot}$  SNe and background from single electron events,  $^{39}\text{Ar}$  decays and external background from SiPMs. Bottom. Time evolution of signal and all background components (external background as expected in Argo) by selecting events in the  $[3,100]$   $N_{e^-}$  energy range.

The expected overall signal-to-background ratio in the GADMC TPCs for the two SN models is  $\sim 24$  and  $\sim 45$ , respectively. In particular, as reported in table 2, the signal is about two orders of magnitude larger than the background during the neutronization burst ( $< 0.02$  s) and the accretion phase ( $[0.02, 1]$  s), while it is about one order of magnitude in the cooling phase ( $[1, 8]$  s), where however the statistic is the largest.

From the same table 2, it can be noticed that the number of events expected from the neutronization burst varies by only 10% between  $11 M_{\odot}$  and  $27 M_{\odot}$  SNe, while those from accretion and cooling phases vary by almost a factor of two. As already suggested in ref. [17], the relatively high statistic measurements of the differential energy and time spectra of the SN with Argo, that will be discussed in section 5, can provide a substantial constraint of SN models and pave the way to the progenitor mass measurement. The sensitivity to the mass is not considered in this work but will be evaluated in the future, once the relationship between progenitor mass and fraction of neutrinos emitted during neutronization will be assessed by theory.

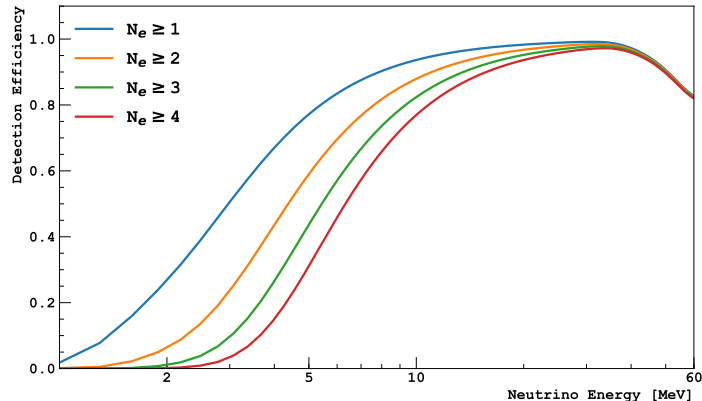


**Figure 4.** Neutrino detection efficiency via CE $\nu$ NS as a function of neutrino energy, for different  $N_{e^-}$  thresholds and below  $100 N_{e^-}$ .

**Table 1.** Event statistics expected in DarkSide-20k and Argo from 11- $M_{\odot}$  and 27- $M_{\odot}$  SNe at 10 kpc and from single-electron and  $^{39}\text{Ar}$  background components, within the  $[3, 100] N_{e^-}$  energy window and in 8 s from the beginning of the burst.

	DarkSide-20k	Argo
11- $M_{\odot}$ SN- $\nu$ s	181.4	1396.6
27- $M_{\odot}$ SN- $\nu$ s	336.5	2591.6
$^{39}\text{Ar}$	4.3	33.8
external background	1.8	8.8
single-electrons	0.7	5.1

**Table 2.** Number of events per unit of mass expected in GADMC TPCs from 11- $M_{\odot}$  and 27- $M_{\odot}$  SNe at 10 kpc and signal-to-background ratio, accounting for single-electron, external background, and  $^{39}\text{Ar}$  rates, within the  $[3, 100] N_{e^-}$  energy window.

SN phase	11- $M_{\odot}$ SN			27- $M_{\odot}$ SN		
	SN- $\nu$ [1/t]	S/B		SN- $\nu$ [1/t]	S/B	
		DS20k	ARGO		DS20k	ARGO
Burst	0.08	212	231	0.09	243	264
Accretion	1.83	105	114	3.30	190	207
Cooling	1.96	16	17	3.76	30	33

## 5 Sensitivity to supernova neutrinos

The background expected in DarkSide-20k and Argo can be assumed to be constant in time and known with negligible uncertainty, as it will be measured with very high statistics before and after the SN burst. This allows to estimate the median significance using the Asimov approximation for likelihood-based tests [38]. The significance for both the TPCs and both the 11- $M_{\odot}$  and 27- $M_{\odot}$  SN models, assuming the background rate from table 1, is shown with solid lines in figure 5, as a function of the SN distance from the Earth. The DarkSide-20k discovery potential entirely covers distances up to the edge of the Milky Way, and Argo extends it up almost to the Small Magellanic Cloud. As shown by the bands in figure 5, the potential increases significantly by assuming lower contamination of  $^{39}\text{Ar}$ , as suggested in the previous section, up to a factor of 10 less. The detection sensitivity can be compared with

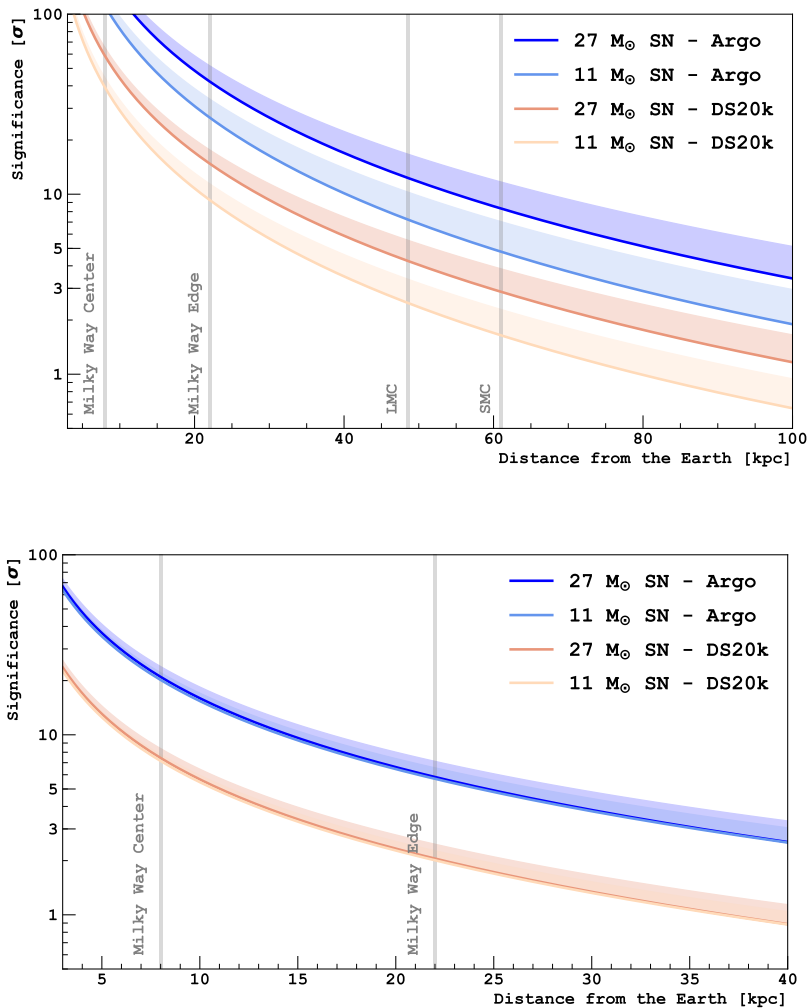


**Figure 5.** Top. DarkSide-20k and Argo significance to 11- $M_{\odot}$  and 27- $M_{\odot}$  SNe (top) and to its neutronization burst only (bottom), as a function of the distance, assuming the standard background hypothesis (solid line) and (band) lower contamination of  $^{39}\text{Ar}$  up to a factor of 10 less. Vertical lines represent the distance from the Earth of the Milky Way center and farthest edge, and of Large (LMC) and Small (SMC) Magellanic Clouds.

the most recent determination of the expected SN core-collapse rate, namely one event every 50 years within 30 kpc inside the Milky Way, and one event every 30 years within 3 Mpc, which includes the Local Group [39–41].

As for the neutralization burst only, DarkSide-20k can detect it as far as 10 kpc with a confidence level of  $5\sigma$ , and Argo can extend it to  $\sim 22$  kpc, a distance equivalent to the farthest edge of the Milky Way from the Earth. In this case, the significance, shown in figure 5, is similar for the two analyzed 11- $M_{\odot}$  and 27- $M_{\odot}$  SN models, as the number of events expected in the neutronization burst differs by only  $\sim 10\%$ .

DarkSide-20k and Argo, besides their use as counting experiments, can also provide information on the time and energy evolution of the neutrino flux. Simulations are performed, using a toy Monte Carlo approach, by applying on an event-by-event basis the detector response described in section 3 to the interaction rate, obtained from the convolution of the



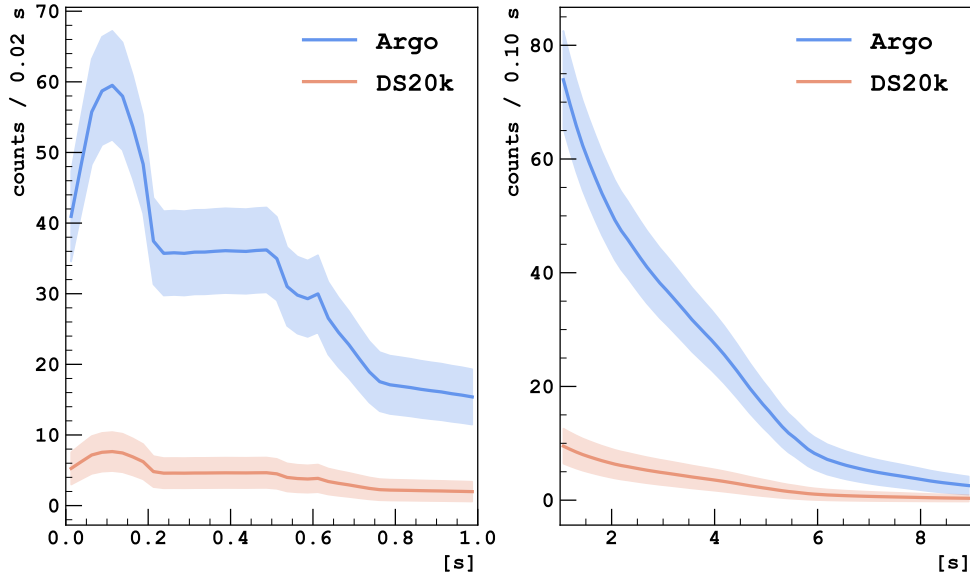


**Figure 6.** Time profile of neutrinos from the accretion (left) and cooling (right) phases of a  $27\text{-}M_{\odot}$  SN at 10 kpc distance, as detected by DarkSide-20k and Argo. The bands represent the statistical uncertainty.

neutrino flux from Garching simulations with the  $\text{CE}\nu\text{NS}$  cross-section (eq. 3.1).

The simulated time evolution of the accretion and cooling phases, as detected with DarkSide-20k and Argo, is shown in figure 6 for a  $27\text{-}M_{\odot}$  SN at 10 kpc. The energy window is limited to  $[3, 100] N_{e^-}$ , where the background is almost entirely suppressed. The statistical error bands of the signal events are evaluated with respect to the sampling of 20 and 100 ms for the two phases, respectively. The detector time responses of DarkSide-20k and Argo, dominated by the associated electron drift times, are included in the simulations. It is worth highlighting that the statistics expected in Argo, together with the time resolution, allows to distinguish the temporal structures that characterize the different SN phases, and therefore to better constrain the models.

Examples of toy Monte Carlo samples in the  $N_{e^-}$  observable for the accretion phase only and for all the SN phases but neutronization burst are shown in figure 7. These samples were produced for Argo, assuming the neutrino flux from a 10 kpc distant  $27\text{-}M_{\odot}$  SN. From now on, we consider only this SN model for the following sensitivity study.

The energy spectrum of the sum of all the SN emitted neutrino components can be parametrized with [42]

$$f(E_{\nu}) = \frac{\xi}{4\pi D^2} \frac{(\alpha_T + 1)^{\alpha_T + 1} E_{\nu}^{\alpha_T} e^{-\frac{E_{\nu}(\alpha_T + 1)}{\langle E_{\nu} \rangle}}}{\langle E_{\nu} \rangle^{\alpha_T + 1} \Gamma(\alpha_T + 1)}, \quad (5.1)$$

where  $E_{\nu}$  is the neutrino energy,  $\xi$  and  $\langle E_{\nu} \rangle$  are the total and mean SN neutrino energies emitted via neutrinos, respectively,  $\alpha_T$  the so-called pinching parameter,  $D$  the distance to the SN, and  $\Gamma$  the Euler gamma function. The spectrum in the neutronization burst can be approximated assuming  $\alpha_T=3.0$ , and with  $\alpha_T=2.3$  in the accretion phase, where the neutrino

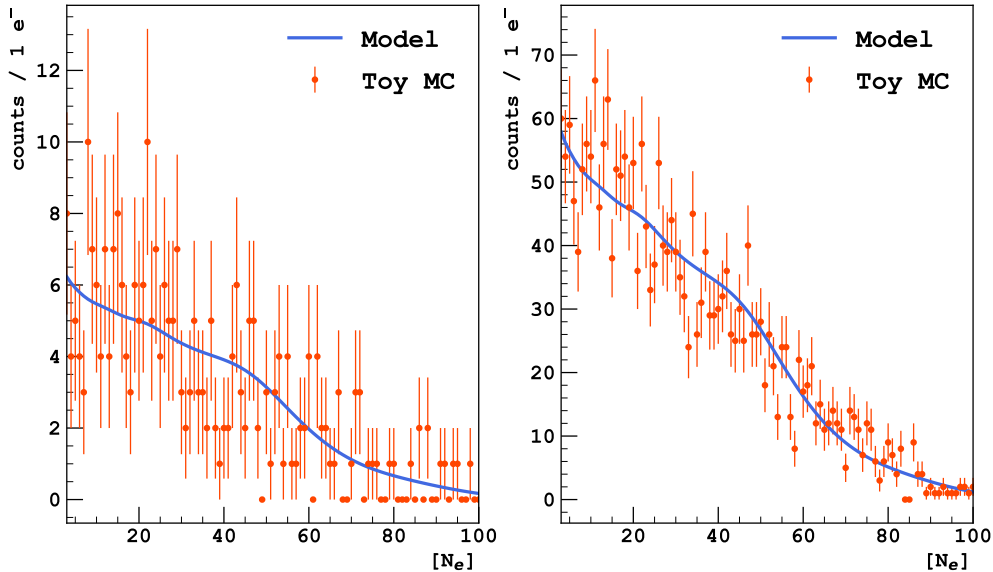


**Figure 7.** Examples of fit of two toy Monte Carlo neutrino interaction samples in DarkSide-20k (left) and Argo (right), generated in the  $[0.02, 8]$  s time range, corresponding to the accretion and cooling phases from a  $27 M_{\odot}$  SN burst at 10 kpc.

emission starts to have a thermal spectrum. In the cooling phase, the neutrino emission is close to having a Maxwell-Boltzmann distribution, where  $\alpha_T=2.0$ .

The parametrized flux in eq. 5.1, convoluted with the  $CE\nu$ NS cross-section and the detector response, is used to fit toy Monte Carlo samples, in order to assess the DarkSide-20k and Argo sensitivities to the total and mean SN neutrino energies. Because of the non-normal fluctuations in the detector response, especially when  $N_{e-}$  is close to the detector threshold ( $3 N_{e-}$ ), the convolution with the detector response is performed using a migration matrix, which transforms nuclear recoil energy into the  $N_{e-}$  response function. This accounts also for the  $N_{e-}$  fluctuations as discussed in section 3. Examples of fits of toy Monte Carlo samples are shown in figure 7.

We have analyzed the two previously mentioned cases: the cooling phase only, and the full SN spectrum, excluding the neutronization burst. This choice is motivated by the good approximation of eq. 5.1 with the accretion phase spectrum, assuming  $\alpha_T=2.3$ , and the similar  $\alpha_T$  value between the accretion and the cooling phase. For the latter case, as the cooling phase provides a larger statistics with respect to the accretion one, we assume  $\alpha_T$  fixed to 2.0. The statistics from the neutronization burst only is too low to allow for a spectral fit. In addition, as already discussed, the pinching parameter is too different from the other phases to allow for an overall approximation with a unique  $\alpha_T$  value.

The sensitivities to  $\langle E_{\nu} \rangle$  and  $\xi$  in the accretion only and accretion+cooling phases are evaluated for both DarkSide-20k and Argo. In each analyzed case, we have produced and fitted  $5 \times 10^4$  samples and derived the significance bands for 1, 2, and 3- $\sigma$  computed from the distribution of the best values from the fit. The results are shown in figure 8, together with the true values extracted from the original Garching simulations.

Both the experiments are able to reconstruct  $\langle E_{\nu} \rangle$  and  $\xi$  within 1- $\sigma$ , even if a systematic shift between true and reconstructed best values is present due to the parametrization

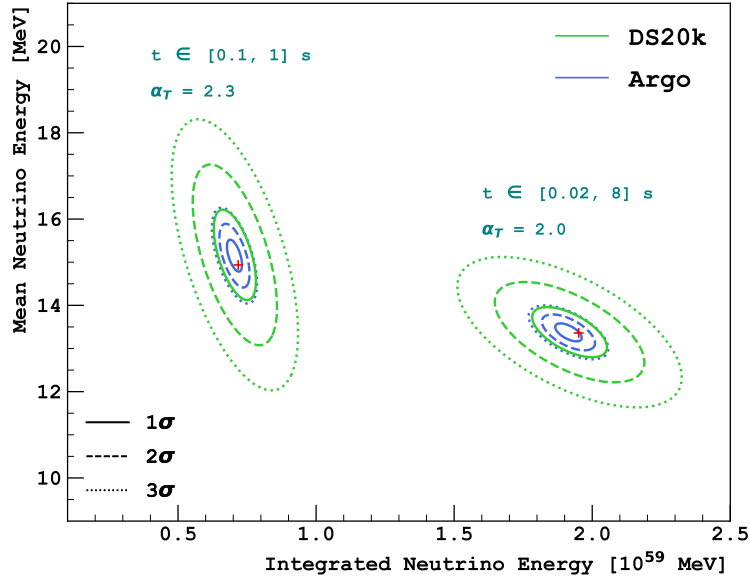


**Figure 8.** DarkSide-20k and Argo sensitivities to mean and integrated neutrino energies of a  $27 M_{\odot}$  SN burst at 10 kpc in the  $[0.1, 1]$  s and  $[0.02, 8]$  s. The two parameters are obtained by fitting  $5 \times 10^4$  toy MC samples with  $\alpha_T$  equals to 2.3 and 2.0, with respect to each time range. Red crosses represent the true values from the Garching simulation.

approximation and the non-normal response of the detector. The total neutrino energy is reconstructed at  $3\text{-}\sigma$  level by Argo (DarkSide-20k) with an accuracy of about 11% (32%) in the accretion-only and 7% (21%) summing the contributions from both accretion and cooling phases. For what concerns the mean energy, Argo has a  $3\text{-}\sigma$  level accuracy at 7% in the accretion phase only, and at 5% including also the cooling one. For the same parameter, DarkSide-20k can provide an accuracy of 21% and 13%, respectively. It is important to stress that the two parameters, as clearly visible in figure 8, are anti-correlated, with a measured Pearson correlation coefficient of about -0.6 for all the analyzed cases.

## 6 Conclusions

DarkSide-20k and Argo, with fiducial target masses of  $\sim 50$  t and  $\sim 360$  t, respectively, can detect neutrinos from SN burst via the flavor-insensitive  $\text{CE}\nu\text{NS}$  channel, with an energy threshold of  $0.46 \text{ keV}_{nr}$ . Such a low analysis energy threshold can be achieved thanks to the  $\sim 20\%$  accuracy in detecting single ionization electrons, as already demonstrated by DarkSide-50.

The low energy threshold, the resolution in the single-electron response, in addition to the light argon nucleus, which, compared to xenon targets, kinematically extends nuclear recoil spectrum at higher energies, provides to GADMC TPCs good accuracy in the reconstruction of average and integrated SN-emitted neutrino energies. Concurrently, the time evolution of SN burst can be investigated with 1.1 ms and 1.6 ms resolutions for DarkSide-20k and Argo, respectively, dominated by the electron drift time in the TPC.

The discovery potential of a SN was also evaluated, demonstrating that DarkSide-20k can explore  $11\text{-}M_{\odot}$  SNe up to the Milky Way edge, and Argo up to the Small Magellanic

Cloud. Both the detectors are also sensitive to neutrinos from the neutronization burst only up to beyond the Milky Way center and edge, respectively, for the same SN model. These results take into account the most conservative predictions of  $^{39}\text{Ar}$  contamination. As already discussed, recent investigations from the DarkSide Collaboration suggest that the  $^{39}\text{Ar}$  contamination, intrinsic to underground argon, could be lower than the DarkSide-50 measured one, leading to a potential further improvement of the DarkSide-20k and Argo sensitivities.

## Acknowledgments

We are grateful to Prof. Alessandro Mirizzi, who provided the input fluxes for this study and invaluable sustain in our discussions on the supernova explosion mechanism. We also thank Mariangela Settimo for the useful comments. The DarkSide Collaboration would like to thank LNGS and its staff for invaluable technical and logistical support. This report is based upon work supported by the U. S. National Science Foundation (NSF) (Grants No. PHY-0919363, No. PHY-1004054, No. PHY-1004072, No. PHY-1242585, No. PHY-1314483, No. PHY-1314507, associated collaborative grants, No. PHY-1211308, No. PHY-1314501, No. PHY-1455351 and No. PHY-1606912, as well as Major Research Instrumentation Grant No. MRI-1429544), the Italian Istituto Nazionale di Fisica Nucleare (Grants from Italian Ministero dell’Istruzione, Università, e Ricerca Progetto Premiale 2013 and Commissione Scientific Nazionale II). We acknowledge the financial support by LabEx UnivEarthS (ANR-10-LABX-0023 and ANR-18-IDEX-0001), the São Paulo Research Foundation (Grant FAPESP-2017/26238-4), and the Russian Science Foundation Grant No. 16-12-10369. The authors were also supported by the “Unidad de Excelencia María de Maeztu: CIEMAT - Física de partículas” (Grant MDM2015-0509), the Polish National Science Centre (Grant No. UMO-2019/33/B/ST2/02884), the Foundation for Polish Science (Grant No. TEAM/2016-2/17), the International Research Agenda Programme AstroCeNT (Grant No. MAB/2018/7) funded by the Foundation for Polish Science from the European Regional Development Fund, the Science and Technology Facilities Council, part of the United Kingdom Research and Innovation, and The Royal Society (United Kingdom). I.F.M.A is supported in part by Conselho Nacional de Desenvolvimento Científico e Tecnológico (CNPq). We also wish to acknowledge the support from Pacific Northwest National Laboratory, which is operated by Battelle for the U.S. Department of Energy under Contract No. DE-AC05-76RL01830.

## References

- [1] A. Burrows, J. Hayes and B. A. Fryxell, *On the nature of core collapse supernova explosions*, *Astrophys. J.* **450** (1995) 830 [[astro-ph/9506061](#)].
- [2] KAMIOKANDE-II collaboration, *Observation of a Neutrino Burst from the Supernova SN 1987a*, *Phys. Rev. Lett.* **58** (1987) 1490.
- [3] IMB collaboration, *Neutrinos From SN1987A in the Imb Detector*, *Nucl. Instrum. Meth. A* **264** (1988) 28.
- [4] E. Alekseev, L. Alekseeva, I. Krivosheina and V. Volchenko, *Detection of the Neutrino Signal From SN1987A in the LMC Using the Inr Baksan Underground Scintillation Telescope*, *Phys. Lett. B* **205** (1988) 209.
- [5] H.-T. Janka, K. Langanke, A. Marek, G. Martinez-Pinedo and B. Mueller, *Theory of Core-Collapse Supernovae*, *Phys. Rept.* **442** 38 [[astro-ph/0612072](#)].

- [6] S. Horiuchi and J. P. Kneller, *What can be learned from a future supernova neutrino detection?*, *J. Phys. G* **45** (2018) 043002 [[1709.01515](#)].
- [7] A. Mirizzi, I. Tamborra, H.-T. Janka, N. Saviano, K. Scholberg, R. Bollig et al., *Supernova Neutrinos: Production, Oscillations and Detection*, *Riv. Nuovo Cim.* **39** (2016) 1 [[1508.00785](#)].
- [8] C. Aalseth et al., *DarkSide-20k: A 20 tonne two-phase LAr TPC for direct dark matter detection at LNGS*, *Eur. Phys. J. Plus* **133** (2018) 131 [[1707.08145](#)].
- [9] COHERENT collaboration, *Observation of Coherent Elastic Neutrino-Nucleus Scattering*, *Science* **357** (2017) 1123 [[1708.01294](#)].
- [10] SUPER-KAMIOKANDE collaboration, *Search for Supernova Neutrino Bursts at Super-Kamiokande*, *Astrophys. J.* **669** 519 [[0706.2283](#)].
- [11] HYPER-KAMIOKANDE WORKING GROUP collaboration, *Neutrino physics perspectives with Hyper-Kamiokande*, *Nucl. Part. Phys. Proc.* **265-266** (2015) 275.
- [12] ICECUBE collaboration, *The IceCube Neutrino Observatory Part V: Neutrino Oscillations and Supernova Searches*, in *33rd International Cosmic Ray Conference*, 9, 2013, [1309.7008](#).
- [13] M. Colomer Molla and M. Lincetto, *Core-Collapse Supernova neutrino detection prospects with the KM3NeT neutrino telescopes.*, *EPJ Web Conf.* **209** (2019) 01009.
- [14] DUNE collaboration, *The DUNE Far Detector Interim Design Report Volume 1: Physics, Technology and Strategies*, [1807.10334](#).
- [15] JUNO collaboration, *Neutrino Physics with JUNO*, *J. Phys. G* **43** (2016) 030401 [[1507.05613](#)].
- [16] K. Scholberg, *Supernova Neutrino Detection*, *Ann. Rev. Nucl. Part. Sci.* **62** (2012) 81 [[1205.6003](#)].
- [17] R. F. Lang, C. McCabe, S. Reichard, M. Selvi and I. Tamborra, *Supernova neutrino physics with xenon dark matter detectors: A timely perspective*, *Phys. Rev. D* **94** (2016) 103009.
- [18] LZ collaboration, *Supernova neutrino detection in LZ*, *JINST* **13** (2018) C02024 [[1801.05651](#)].
- [19] H. T. Janka, *Conditions for shock revival by neutrino heating in core collapse supernovae*, *Astron. Astrophys.* **368** (2001) 527 [[astro-ph/0008432](#)].
- [20] S. W. Bruenn, A. Mezzacappa, W. Hix, E. J. Lentz, O. Messer, E. J. Lingerfelt et al., *Axisymmetric Ab Initio Core-Collapse Supernova Simulations of 12-25 M<sub>⊙</sub> Stars*, *Astrophys. J. Lett.* **767** (2013) L6 [[1212.1747](#)].
- [21] S. Bruenn, A. Mezzacappa, W. Hix, J. Blondin, P. Marronetti, O. Messer et al., *Mechanisms of Core-Collapse Supernovae & Simulation Results from the CHIMERA Code*, vol. 1111, p. 593, 2009, [1002.4909](#), DOI.
- [22] S. Mikheev and A. Smirnov, *Resonant amplification of neutrino oscillations in matter and solar neutrino spectroscopy*, *Nuovo Cim. C* **9** (1986) 17.
- [23] H. Duan, G. M. Fuller, J. Carlson and Y.-Z. Qian, *Neutrino Mass Hierarchy and Stepwise Spectral Swapping of Supernova Neutrino Flavors*, *Phys. Rev. Lett.* **99** (2007) 241802 [[0707.0290](#)].
- [24] C. Lunardini and A. Y. Smirnov, *Probing the neutrino mass hierarchy and the 13 mixing with supernovae*, *JCAP* **06** (2003) 009 [[hep-ph/0302033](#)].
- [25] I. Tamborra, F. Hanke, B. Müller, H.-T. Janka and G. Raffelt, *Neutrino signature of supernova hydrodynamical instabilities in three dimensions*, *Phys. Rev. Lett.* **111** (2013) 121104 [[1307.7936](#)].
- [26] H.-Y. Chiu and P. Morrison, *Neutrino Emission from Black-Body Radiation at High Stellar Temperatures*, *Phys. Rev. Lett.* **5** (1960) 573.

- [27] L. Hüdepohl, *Neutrinos from the Formation, Cooling, and Black Hole Collapse of Neutron Stars*, dissertation, Technische Universität München, München, 2014.
- [28] “The Garching Core-Collapse Supernova Data Archive.”  
<https://wwwmpa.mpa-garching.mpg.de/ccsnarchive/index.html>.
- [29] J. Lewin and P. Smith, *Review of mathematics, numerical factors, and corrections for dark matter experiments based on elastic nuclear recoil*, *Astropart. Phys.* **6** (1996) 87.
- [30] DARKSIDE collaboration, *Low-Mass Dark Matter Search with the DarkSide-50 Experiment*, *Phys. Rev. Lett.* **121** (2018) 081307 [[1802.06994](#)].
- [31] P. Agnes et al., *Measurement of the liquid argon energy response to nuclear and electronic recoils*, *Phys. Rev. D* **97** (2018) 112005 [[1801.06653](#)].
- [32] SCENE collaboration, *Measurement of Scintillation and Ionization Yield and Scintillation Pulse Shape from Nuclear Recoils in Liquid Argon*, *Phys. Rev. D* **91** (2015) 092007 [[1406.4825](#)].
- [33] J. Thomas and D. A. Imel, *Recombination of electron-ion pairs in liquid argon and liquid xenon*, *Phys. Rev. A* **36** (1987) 614.
- [34] DARKSIDE collaboration, *Constraints on Sub-GeV Dark-Matter–Electron Scattering from the DarkSide-50 Experiment*, *Phys. Rev. Lett.* **121** (2018) 111303 [[1802.06998](#)].
- [35] DARKSIDE collaboration, *Simulation of argon response and light detection in the DarkSide-50 dual phase TPC*, *JINST* **12** (2017) P10015 [[1707.05630](#)].
- [36] GLOBAL ARGON DARK MATTER collaboration, “Future dark matter searches with low-radioactivity argon.” [European Strategy Update](#), 2018.
- [37] DARKSIDE collaboration, *Electroluminescence pulse shape and electron diffusion in liquid argon measured in a dual-phase TPC*, *Nucl. Instrum. Meth. A* **904** (2018) 23 [[1802.01427](#)].
- [38] G. Cowan, K. Cranmer, E. Gross and O. Vitells, *Asymptotic formulae for likelihood-based tests of new physics*, *Eur. Phys. J. C* **71** (2011) 1554 [[1007.1727](#)].
- [39] E. Cappellaro, R. Evans and M. Turatto, *A new determination of supernova rates and a comparison with indicators for galactic star formation*, *Astron. Astrophys.* **351** (1999) 459 [[astro-ph/9904225](#)].
- [40] W. Li, A. V. Filippenko, R. Treffers, A. Riess, J. Hu and Y. Qiu, *A high intrinsic peculiarity rate among type Ia supernovae*, *Astrophys. J.* **546** (2001) 734 [[astro-ph/0006292](#)].
- [41] M. Botticella et al., *Supernova rates from the SUDARE VST-Omegacam search II. Rates in a galaxy sample*, *Astron. Astrophys.* **598** (2017) A50 [[1610.01176](#)].
- [42] M. T. Keil, G. G. Raffelt and H.-T. Janka, *Monte Carlo study of supernova neutrino spectra formation*, *Astrophys. J.* **590** (2003) 971 [[astro-ph/0208035](#)].